Three-Dimensional Carbon-Honeycomb as Nanoporous Lithium and Sodium Deposition Scaffold
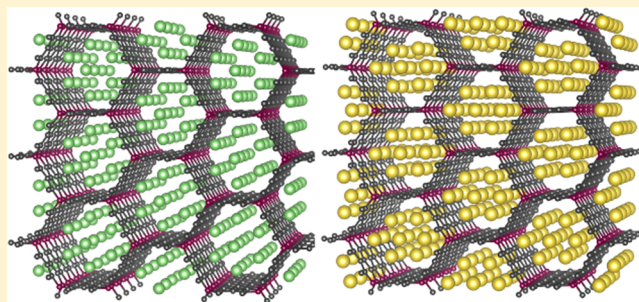
Le Shi, Ao Xu, and Tianshou Zhao*

HKUST Energy Institute, Department of Mechanical and Aerospace Engineering, The Hong Kong University of Science and Technology, Hong Kong 999077, China

Ⓢ Supporting Information

ABSTRACT: Using the density functional theory method, we demonstrate that the recently synthesized three-dimensional carbon-honeycomb (C-honeycomb) can serve as a promising nanoporous scaffold for both lithium and sodium deposition with good electronic conductivity. Lithium/sodium can insert into the channels of C-honeycomb with low migration energy barriers along the walls of one-dimensional pores (<0.5 eV for lithium and <0.25 eV for sodium) and exist in the form of metal nanorods. A high theoretical capacity (711 mAh/g, almost twice that of graphite) can be achieved when the one-dimensional pores are filled with lithium/sodium atoms. The volume expansion of the C-honeycomb after metal insertion is less than 5 and 15% for lithium and sodium, respectively. Further introduction of defects such as pyridinic-N doping or single vacancy can provide initial nucleation sites for the metal nanorods and increase the open-circuit voltage.

1. INTRODUCTION

Along with the development of lithium-based batteries, conventional graphite anodes can no longer provide satisfactory performance due to their low theoretical capacity (372 mAh/g).[1] New anode materials with higher capacity, such as silicon and tin, have been proposed and have attracted considerable attention in recent years.[2−5] However, as the lithium atoms are stored based on an alloy mechanism, these anode materials suffer from severe volume expansion when providing high capacity, which can cause pulverization of the anode materials and seriously lower the cycle performance. Employment of nanomaterials[6−10] can significantly alleviate the volume expansion and provide a longer cycle life, but the resulting volumetric energy density will be much lower and a large amount of solid electrolyte interphase will be formed due to the large surface area. Therefore, three-dimensional (3D) bulk materials, which can provide high capacity, good electronic conductivity, and small volume expansion, will be the ideal candidates for lithium anodes. On the other hand, sodium-based batteries have been regarded as promising alternatives for lithium-based batteries due to the abundance and low cost of the sodium element.[11−15] Due to the larger atom size, sodium can hardly intercalate into the graphite interlayers and the corresponding capacity is lower than 50 mAh/g.[11] Other possible anode materials, such as phosphorus, suffer from the same problem of large volume expansion as that of alloy-based lithium anode materials.[16−20] Thus, a new sodium anode material with high capacity and small volume expansion is urgently needed.

In addition to graphite, various kinds of three-dimensional carbon structures, such as T6- and T14-carbon,[21] interpenetration graphene networks,[22] 16-atom body-centered orthorhombic unit cells (bco-C$_{16}$),[23] and Hex-C$_{18}$,[24] have been predicted based on ab initio calculations. Recently, Krainyukova et al.[25] have successfully synthesized a new stable allotrope of carbon, named carbon honeycomb (C-honeycomb, C-h), via deposition of vacuum-sublimated graphite. Later, theoretical calculations[26−29] confirmed that the stable C-honeycomb structure is composed of graphene nanoribbons connected by sp^3 carbon atoms as junctions, as shown in Figure 1. The C-honeycomb exhibits superior mechanical and thermal properties, and the aligned one-dimensional (1D) channels in the C-honeycomb make it a promising material for gas adsorption[25] and lithium/sodium storage. As the radius of the 1D channels of the C-honeycomb is much larger than the interlayer spacing of graphite, we propose that different from graphite, where lithium atoms intercalate between the interlayers and exist as separated atoms, lithium/sodium atoms may insert into the 1D channels and nucleate into metal nanorods, thus providing a much higher capacity. The C-honeycomb can be regarded as a nanoporous lithium/sodium deposition scaffold. Its nanoscale pore size makes it much safer than the microporous lithio/sodiophilic frameworks,[30−33] in which lithium/sodium can form a large-scale continuous phase.
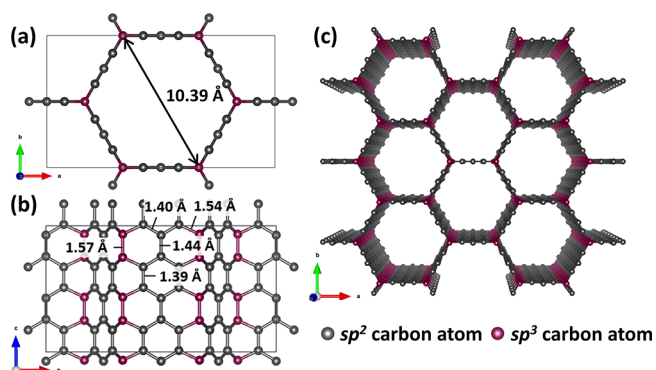
Figure 1. Geometry of C-honeycomb from (a) side, (b) top, and (c) perspective views.

2. COMPUTATIONAL METHODOLOGY

All the computations were performed using the Abinit[34−36] software package with the Perdew−Burke−Ernzerhof generalized gradient approximation[37] and the projector augmented wave method.[38] Grimme's DFT-D2[39] correction was adopted to account for the van der Waals interaction. The cutoff energy was set to be 20 Ha. The k-point mesh was set to be <0.06 Å^{-1} for geometry optimization and <0.03 Å^{-1} for the calculation of density of states. All of the structures were fully optimized to a force tolerance of 0.01 eV/Å. The migration energy barriers of lithium/sodium inside the C-honeycomb were calculated using the climbing image nudged elastic band method,[40] and 15 images were used. The binding energies were calculated as[41]

$$E_{bind} = (E_{C\text{-}h+M} - E_{C\text{-}h} - n\mu_M)/n \tag{1}$$

and the adsorption energies were calculated as

$$E_{ads} = (E_{C\text{-}h+M} - E_{C\text{-}h} - nE_M)/n \tag{2}$$

where $E_{C\text{-}h+M}$ is the total energy of lithium/sodium atoms adsorbed on the C-honeycomb, $E_{C\text{-}h}$ is the total energy of the C-honeycomb, n is the number of lithium/sodium atoms adsorbed, μ_M is the chemical potential of metallic lithium/ sodium atom, and E_M is the energy of a single lithium/sodium atom. The open-circuit voltage (OCV) was estimated by[41]

$$OCV \approx [E_{Mx_1C\text{-}h} - E_{Mx_2C\text{-}h} + (x_2 - x_1)\mu_M]/(x_2 - x_1)e \tag{3}$$

where $E_{Mx_1C\text{-}h}$ and $E_{Mx_2C\text{-}h}$ denote the total energy of the C-honeycomb adsorbed with x_1 and x_2 lithium/sodium atoms.

3. RESULTS AND DISCUSSION

3.1. Geometry and Electronic Conductivity of Carbon-Honeycomb. We optimized the geometry of the C-honeycomb based on the structure proposed by Pang et al.,[26] and the 6-6-6 sp^3 junction was chosen instead of the 5-5-8 junction owing to its lower cohesive energy.[26,27] A $1 \times 1 \times 2$ supercell consisting of 88 carbon atoms was adopted for further calculations. The detailed geometry of the optimized C-honeycomb is shown in Figure 1, and the diameter of the 1D channels is about 1 nm. In addition to the pristine C-honeycomb, the C-honeycomb may also accommodate the same type of defects as graphene at low energy cost as predicted by Zhu and Tománek.[42] Thus, we further considered the influence of pyridinic-N doping and formation of single vacancy toward the performance of C-honeycomb as anode material (illustrated in Figure 2a1,a2). The calculated density of states in Figure 2b shows that the pristine C-honeycomb exhibits a small band gap of about 0.5 eV, while after the introduction of pyridinic-N doping or single vacancy, the density of states at the Fermi level becomes a positive value, which indicates better electronic conductivity. These results ensure that the C-honeycomb can provide sufficient electronic conductivity when serving as lithium/sodium anode material.
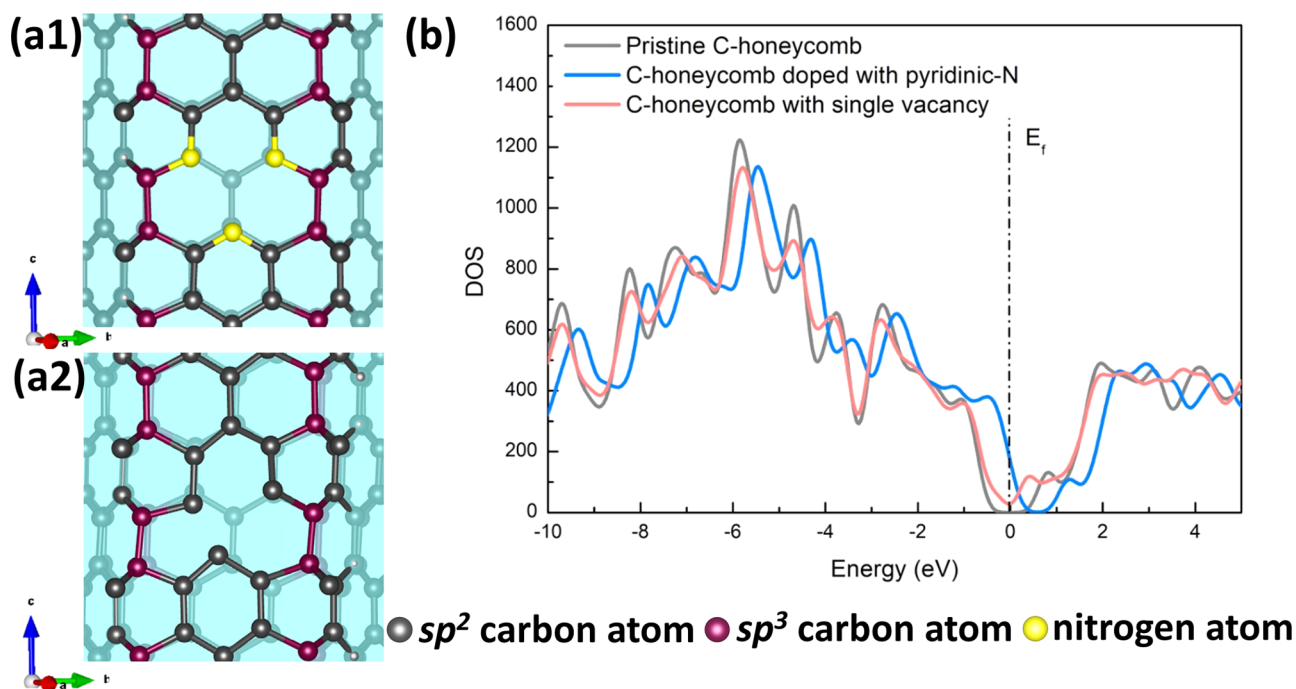

Figure 2. Geometry of (a1) pyridinic-N doping and (a2) single vacancy. (b) Density of states of pristine C-honeycomb, C-honeycomb doped with pyridinic-N, and C-honeycomb with single vacancy, where the dashed line represents the Fermi level.
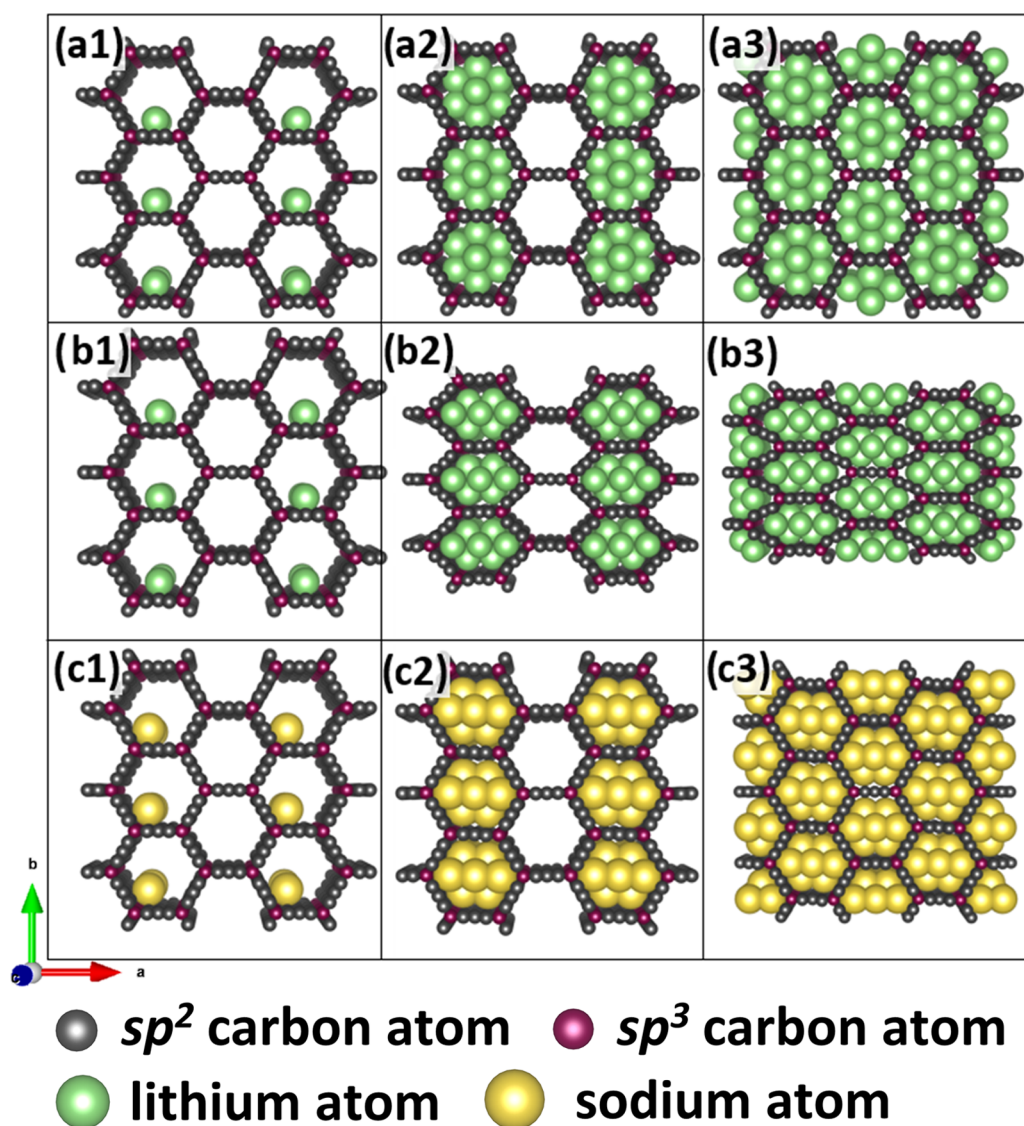
● *sp²* carbon atom　　● *sp³* carbon atom
● lithium atom　　● sodium atom

Figure 3. Perspective view of a $1 \times 1 \times 2$ pristine C-honeycomb supercell filled with (a1)−(a3) 1, 14, and 28 lithium atoms packed in hexagonal form; (b1)−(b3) 1, 14, and 28 lithium atoms packed in cubic form; and (c1)−(c3) 1, 14, and 28 sodium atoms packed in cubic form.

3.2. Lithium/Sodium Insertion into Carbon-Honeycomb. The binding energies of lithium/sodium at different concentrations on the C-honeycomb were calculated. For a single lithium/sodium atom, several possible lithium/sodium adsorption sites on the pristine C-honeycomb were studied, as shown in Figure S2. From the binding energies listed in Table S2, the interactions between lithium/sodium atoms and C-honeycomb are relatively weak and the binding energies are positive, similar to the case of pristine graphene.[43] Then, we tried to increase the lithium/sodium insertion concentration. On the basis of the size of the nanochannel, the highest amount of lithium/sodium that can be inserted is (Li/Na)$_{28}$C$_{88}$, corresponding to a capacity of 711 mAh/g. Two packing forms of lithium/sodium inside the channels were considered. The first one, named "hexagonal form", was constructed based on the most stable single-atom adsorption site, where six lithium/sodium atoms were attached to their most stable adsorption site on the wall, then another lithium/sodium atom is ahead of the hexagonal ring formed, as shown in Figure S3a. The second one, named "cubic form", was constructed based on the bulk structure of lithium/sodium

metal, where the lithium/sodium atoms were packed in the same way as their bulk form, as shown in Figure S3b,c. After geometrical optimization, the hexagonal packing form becomes unstable for sodium and will transform into cubic form during the structural optimization process. The perspective view of C-honeycomb after 50 and 100% lithium/sodium insertion is shown in Figure 3. For lithium packed in cubic form inside the C-honeycomb, the latter will undergo a significant structural deformation, where the C-honeycomb lattice parallel to the direction packed with more lithium atoms will elongate. As shown in Figure 4, after the insertion of 50% lithium/sodium, the binding energies will be reduced compared to the single-atom cases, and the lithium binding energy will become negative, suggesting that the insertion of lithium into the C-honeycomb channels at high concentration is thermodynamically favorable compared to forming a segregated lithium phase. After the insertion of 100% lithium/sodium, the binding energies will be further reduced and the sodium binding energy will become very close to zero (+0.01 eV). The reduced binding energy comes from the cohesive energy of metal packing, and the cubic form packing is more stable compared
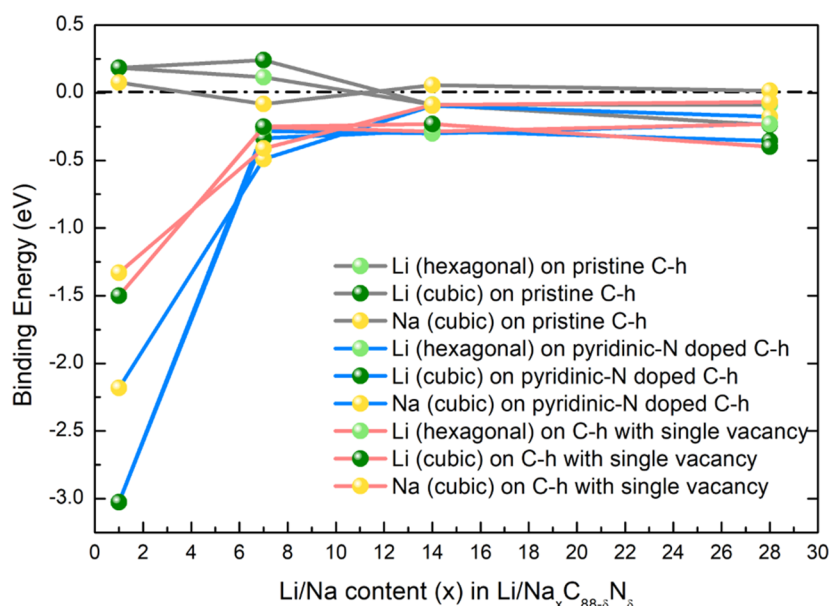
Figure 4. Binding energies of lithium/sodium onto pristine and defective C-honeycomb (C-h) at different concentrations.
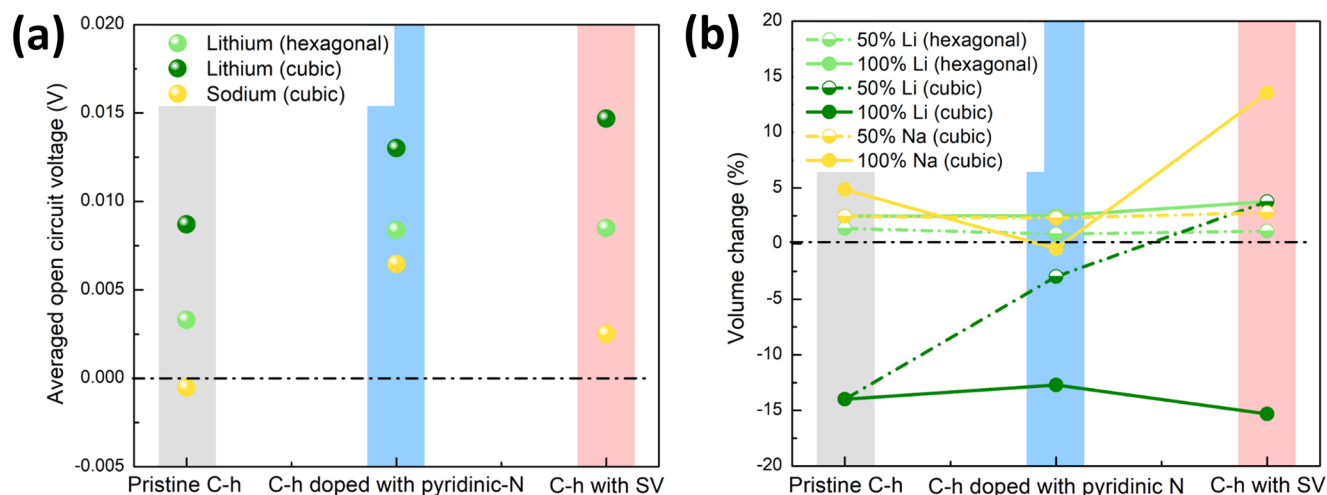

Figure 5. (a) Averaged open-circuit voltage of pristine C-honeycomb (C-h), C-honeycomb doped with pyridinic-N, and C-honeycomb with single vacancy as the anode material for lithium- and sodium-ion batteries (b) volume change of pristine C-honeycomb, C-honeycomb doped with pyridinic-N, and C-honeycomb with single vacancy when filled with 50 and 100% lithium or sodium atoms. The symbols in (b) were linked to guide the eye.

to the hexagonal form, thus contributing to more cohesive energy and resulting in lower binding energy.

The pristine C-honeycomb can provide negative binding energies toward lithium at high concentrations, but cannot stabilize the adsorption of a single lithium atom and sodium atoms at all concentrations. Introduction of defects such as nitrogen doping or vacancy has been proven to be an effective strategy to enhance the interaction between metal atoms and graphene basal plane.[44−46] Therefore, we start to study the lithium/sodium binding onto the defective C-honeycomb. In addition to the pyridinic-N doping and single vacancy mentioned above, graphitic-N doping was also studied as shown in Figure S4. However, from the calculated binding energies as listed in Table S3, the graphitic-N doping shows little influence toward the binding energies; thus, it is not considered for further discussions. The other form of reported N doping, the pyrrolic-N doping, requires larger graphene nanoribbons and cannot be properly constructed in our case.[47]

Figures S6−S11 show the geometries of lithium/sodium insertion inside C-honeycomb with pyridinic-N doping and single vacancy. The most stable binding site will change due to the introduction of defects, and the packing form will be altered slightly. Figure S12 shows the electron distribution of C-honeycomb doped with pyridinic-N and C-honeycomb with single vacancy. It is found that the introduction of these defects creates an electron-deficient area in the C-honeycomb, which can help trap the lithium/sodium atoms. Figures S13 and S14 show the charge transfer between adsorbed lithium/sodium atoms and pristine C-honeycomb, C-honeycomb doped with pyridinic-N, and C-honeycombs with single vacancy. It is found that the area involved in the charge-transfer process becomes larger after the introduction of pyridinic-N doping and single vacancy, which may explain the stronger adsorption behavior.

The binding energies of lithium/sodium on defective C-honeycomb at different concentrations can be found in Figure
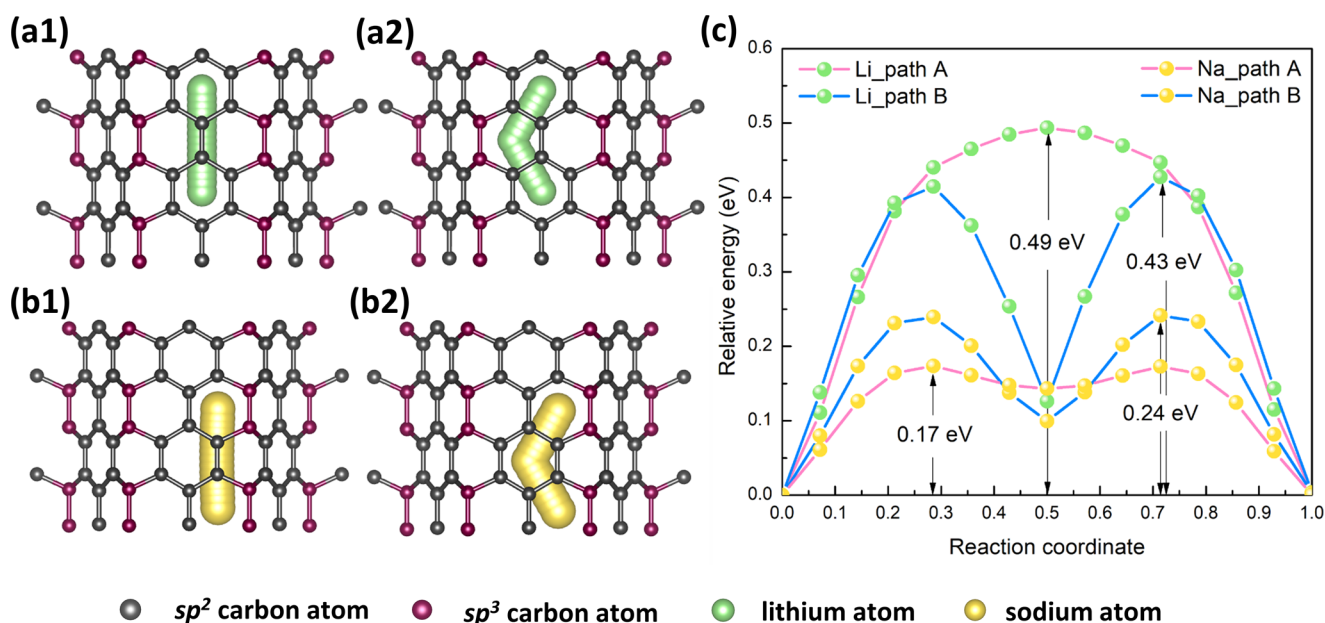
Figure 6. Lithium migration along C-honeycomb channels following (a1) path A and (a2) path B; sodium migration along C-honeycomb following (b1) path A and (b2) path B. (c) Migration energy barriers for lithium/sodium in C-honeycomb.

4. For a single lithium/sodium atom, the binding energy will be greatly lowered after the introduction of pyridinic-N doping or single vacancy. With more lithium/sodium inserted, the influence of defects will be averaged, making the binding energies higher but still negative. These results show that the introduction of defects such as pyridinic-N doping or single vacancy is necessary to lure the lithium/sodium atoms to be inserted into the C-honeycomb channels. Afterward, the inserted lithium/sodium atoms will be trapped on the defect sites and serve as nucleation sites for metal nanorod growth. A small number of defects (3.4% pyridinic-N doping or 1.1% single vacancy) can ensure that the whole insertion process is thermodynamically favorable, which can be realized in experiments easily.[48−53]

The calculated averaged open-circuit voltage (OCV) of pristine and defective C-honeycomb is shown in Figure 5a. Except in the case of sodium in pristine C-honeycomb, all of the OCVs are small positive values, which is similar to that of graphite.[54] The small positive OCVs will ensure the insertion of lithium/sodium inside the C-honeycomb channels and provide a large cell voltage. The volume expansion after lithium/sodium insertion is shown in Figure 5b. For lithium packed in hexagonal form, the volume shows a very slight change within 5%, while for lithium packed in cubic form, the volume shrinks about 15% when the channels are fully filled due to the structural deformation mentioned above. For sodium, the volume expansion is within 15% for all of the cases. The detailed lattice parameter changes can be found in Figures S15−S20.

3.3. Lithium/Sodium Migration Inside Carbon-Honeycomb. We then calculated the migration energy barriers of lithium and sodium inside the channels of C-honeycomb. Two migration pathways were considered for both cases, as shown in Figure 6a,b, path A is that the lithium/sodium atom directly migrates from one most stable adsorption site to the next most stable adsorption site (wall1 → wall1 for lithium and wall2 → wall2 for sodium), and path B is that the lithium/sodium first migrates to the nearest metastable adsorption site and then

migrates to the other most stable adsorption site (wall1 → wall2 → wall1 for lithium and wall2 → wall1 → wall2 for sodium). From Figure 6c, the migration energy barriers are smaller than 0.5 eV for lithium and smaller than 0.25 eV for sodium, similar to our previous results on lithium/sodium migration energy barriers on pristine graphene.[43] These small energy barriers indicate that lithium/sodium atoms can migrate fast inside the 1D channels during the discharge/charge process, thus providing good rate capability.

It is worth mentioning that in addition to the C-honeycomb structure discussed in this work, there exist many other kinds of possible 3D carbon network structures made up of graphene nanoribbon arrays and junctions.[55−58] We expect that these 3D carbon networks share similar electrochemical properties to the C-honeycomb discussed here when serving as lithium/sodium anode materials. Moreover, with a larger pore radius, the theoretical capacity can be further increased and the binding energies at high lithium/sodium concentrations can be further lowered.

4. CONCLUSIONS

In conclusion, we explored the feasibility of using the recently synthesized C-honeycomb as nanoporous scaffold for lithium/sodium deposition using the density functional theory method. Calculation results show that lithium/sodium can insert into the 1D channels of C-honeycomb with low migration energy barriers and be packed inside as metal nanorods, thus providing a high capacity of 711 mAh/g. Introduction of defects such as pyridinic-N doping or single vacancy can significantly lower the binding energies at low lithium/sodium concentrations and provide nucleation sites for further lithium/sodium insertion. Other possible 3D carbon networks sharing a similar structure to C-honeycomb may also be promising lithium/sodium anode materials with even higher capacity depending on their pore size. We hope that these results will provide a new direction to the search of lithium/sodium anode materials.

■ ASSOCIATED CONTENT

Ⓢ Supporting Information

The Supporting Information is available free of charge on the ACS Publications website at DOI: 10.1021/acs.jpcc.8b07691.

Geometry of considered pyridinic-N and single vacancy defects; adsorption sites of pristine C-honeycomb for lithium/sodium; binding energies and adsorption energies of lithium/sodium (PDF)

■ AUTHOR INFORMATION

Corresponding Author

*E-mail: metzhao@ust.hk. Tel: (852) 2358 8647.

ORCID 🌐

Le Shi: 0000-0003-1468-4549
Ao Xu: 0000-0003-0648-2701
Tianshou Zhao: 0000-0003-4825-2381

Notes

The authors declare no competing financial interest.

■ ACKNOWLEDGMENTS

■ REFERENCES

(1) Wu, Y. P.; Rahm, E.; Holze, R. Carbon Anode Materials for Lithium Ion Batteries. *J. Power Sources* **2003**, *114*, 228−236.
(2) Zhang, W. J. A Review of the Electrochemical Performance of Alloy Anodes for Lithium-Ion Batteries. *J. Power Sources* **2011**, *196*, 13−24.
(3) Scrosati, B.; Hassoun, J.; Sun, Y. K. Lithium-Ion Batteries. A Look into the Future. *Energy Environ. Sci.* **2011**, *4*, 3287−3295.
(4) Wachtler, M.; Besenhard, J. O.; Winter, M. Tin and Tin-Based Intermetallics as New Anode Materials for Lithium-Ion Cells. *J. Power Sources* **2001**, *94*, 189−193.
(5) Zhang, W. J. Lithium Insertion/Extraction Mechanism in Alloy Anodes for Lithium-Ion Batteries. *J. Power Sources* **2011**, *196*, 877−885.
(6) Shi, L.; Zhao, T. Recent Advances in Inorganic 2D Materials and Their Applications in Lithium and Sodium Batteries. *J. Mater. Chem. A* **2017**, *5*, 3735−3758.
(7) Magasinski, A.; Dixon, P.; Hertzberg, B.; Kvit, A.; Ayala, J.; Yushin, G. High-Performance Lithium-Ion Anodes Using A Hierarchical Bottom-Up Approach. *Nat. Mater.* **2010**, *9*, 353.
(8) Zhang, W. M.; Hu, J. S.; Guo, Y. G.; Zheng, S. F.; Zhong, L. S.; Song, W. G.; Wan, L. J. Tin-Nanoparticles Encapsulated in Elastic Hollow Carbon Spheres for High-Performance Anode Material in Lithium-Ion Batteries. *Adv. Mater.* **2008**, *20*, 1160−1165.
(9) Zhou, J.; Qin, J.; Zhang, X.; Shi, C.; Liu, E.; Li, J.; Zhao, N.; He, C. 2D Space-Confined Synthesis of Few-Layer MoS₂ Anchored on Carbon Nanosheet for Lithium-Ion Battery Anode. *ACS Nano* **2015**, *9*, 3837−3848.
(10) Qin, J.; He, C.; Zhao, N.; Wang, Z.; Shi, C.; Liu, E. Z.; Li, J. Graphene Networks Anchored with Sn@ Graphene as Lithium Ion Battery Anode. *ACS Nano* **2014**, *8*, 1728−1738.
(11) Slater, M. D.; Kim, D.; Lee, E.; Johnson, C. S. Sodium-Ion Batteries. *Adv. Funct. Mater.* **2013**, *23*, 947−958.
(12) Ellis, B. L.; Nazar, L. F. Sodium and Sodium-Ion Energy Storage Batteries. *Curr. Opin. Solid State Mater. Sci.* **2012**, *16*, 168−177.
(13) Yabuuchi, N.; Kubota, K.; Dahbi, M.; Komaba, S. Research Development on Sodium-Ion Batteries. *Chem. Rev.* **2014**, *114*, 11636−11682.

(14) Xin, S.; Yin, Y. X.; Guo, Y. G.; Wan, L. J. A High-Energy Room-Temperature Sodium-Sulfur Battery. *Adv. Mater.* **2014**, *26*, 1261−1265.
(15) Das, S. K.; Lau, S.; Archer, L. A. Sodium−Oxygen Batteries: A New Class of Metal−Air Batteries. *J. Mater. Chem. A* **2014**, *2*, 12623−12629.
(16) Qian, J.; Wu, X.; Cao, Y.; Ai, X.; Yang, H. High Capacity and Rate Capability of Amorphous Phosphorus for Sodium Ion Batteries. *Angew. Chem., Int. Ed.* **2013**, *125*, 4731−4734.
(17) Zhu, Y.; Wen, Y.; Fan, X.; Gao, T.; Han, F.; Luo, C.; Liou, S. C.; Wang, C. Red Phosphorus−Single-Walled Carbon Nanotube Composite as A Superior Anode for Sodium Ion Batteries. *ACS Nano* **2015**, *9*, 3254−3264.
(18) Zhang, C.; Wang, X.; Liang, Q.; Liu, X.; Weng, Q.; Liu, J.; Yang, Y.; Dai, Z.; Ding, K.; Bando, Y.; Tang, J.; Golberg, D. Amorphous Phosphorus/Nitrogen-Doped Graphene Paper for Ultra-stable Sodium-Ion Batteries. *Nano Lett.* **2016**, *16*, 2054−2060.
(19) Shi, L.; Zhao, T.; Xu, A.; Xu, J. Ab Initio Prediction of Borophene as An Extraordinary Anode Material Exhibiting Ultrafast Directional Sodium Diffusion for Sodium-Based Batteries. *Sci. Bull.* **2016**, *61*, 1138−1144.
(20) Sun, J.; Lee, H. W.; Pasta, M.; Yuan, H.; Zheng, G.; Sun, Y.; Li, Y.; Cui, Y. A Phosphorene−Graphene Hybrid Material as A High-Capacity Anode for Sodium-Ion Batteries. *Nat. Nanotechnol.* **2015**, *10*, 980.
(21) Zhang, S.; Wang, Q.; Chen, X.; Jena, P. Stable Three-Dimensional Metallic Carbon with Interlocking Hexagons. *Proc. Natl. Acad. Sci. U.S.A.* **2013**, *110*, 18809−18813.
(22) Chen, Y.; Xie, Y.; Yang, S. A.; Pan, H.; Zhang, F.; Cohen, M. L.; Zhang, S. Nanostructured Carbon Allotropes with Weyl-like Loops and Points. *Nano Lett.* **2015**, *15*, 6974−6978.
(23) Wang, J. T.; Weng, H.; Nie, S.; Fang, Z.; Kawazoe, Y.; Chen, C. Body-Centered Orthorhombic C₁₆: A Novel Topological Node-Line Semimetal. *Phys. Rev. Lett.* **2016**, *116*, No. 195501.
(24) Liu, J.; Zhao, T.; Zhang, S.; Wang, Q. A New Metallic Carbon Allotrope with High Stability and Potential for Lithium Ion Battery Anode Material. *Nano Energy* **2017**, *38*, 263−270.
(25) Krainyukova, N. V.; Zubarev, E. N. Carbon Honeycomb High Capacity Storage for Gaseous and Liquid Species. *Phys. Rev. Lett.* **2016**, *116*, No. 055501.
(26) Pang, Z.; Gu, X.; Wei, Y.; Yang, R.; Dresselhaus, M. S. Bottom-Up Design of Three-Dimensional Carbon-Honeycomb with Superb Specific Strength and High Thermal Conductivity. *Nano Lett.* **2017**, *17*, 179−185.
(27) Gu, X.; Pang, Z.; Wei, Y.; Yang, R. On the Influence of Junction Structures on the Mechanical and Thermal Properties of Carbon Honeycombs. *Carbon* **2017**, *119*, 278−286.
(28) Gao, Y.; Chen, Y.; Zhong, C.; Zhang, Z.; Xie, Y.; Zhang, S. Electron and Phonon Properties and Gas Storage in Carbon Honeycombs. *Nanoscale* **2016**, *8*, 12863−12868.
(29) Fthenakis, Z. G. Are the Experimentally Observed 3-Dimensional Carbon Honeycombs All-sp² Structures? The Dangling p-Orbital Instability. *RSC Adv.* **2017**, *7*, 9790−9794.
(30) Zhang, R.; Li, N. W.; Cheng, X. B.; Yin, Y. X.; Zhang, Q.; Guo, Y. G. Advanced Micro/Nanostructures for Lithium Metal Anodes. *Adv. Sci.* **2017**, *4*, No. 1600445.
(31) Chi, S. S.; Qi, X. G.; Hu, Y. S.; Fan, L. Z. 3D Flexible Carbon Felt Host for Highly Stable Sodium Metal Anodes. *Adv. Energy Mater.* **2018**, No. 1702764.
(32) Zhu, M.; Li, B.; Li, S.; Du, Z.; Gong, Y.; Yang, S. Dendrite-Free Metallic Lithium in Lithiophilic Carbonized Metal-Organic Frame-works. *Adv. Energy Mater.* **2018**, No. 1703505.
(33) Zhang, R.; Chen, X. R.; Chen, X.; Cheng, X. B.; Zhang, X. Q.; Yan, C.; Zhang, Q. Lithiophilic Sites in Doped Graphene Guide Uniform Lithium Nucleation for Dendrite-Free Lithium Metal Anodes. *Angew. Chem., Int. Ed.* **2017**, *56*, 7764−7768.
(34) Gonze, X.; Beuken, J. M.; Caracas, R.; Detraux, F.; Fuchs, M.; Rignanese, G. M.; Sindic, L.; Verstraete, M.; Zerah, G.; Jollet, F.; Torrent, M.; et al. First-Principles Computation of Material

Properties: the ABINIT Software Project. *Comput. Mater. Sci.* **2002**, *25*, 478−492.

(35) Gonze, X.; Amadon, B.; Anglade, P. M.; Beuken, J. M.; Bottin, F.; Boulanger, P.; Bruneval, F.; Caliste, D.; Caracas, R.; Côté, M.; Deutsch, T.; et al. ABINIT: First-Principles Approach to Material and Nanosystem Properties. *Comput. Phys. Commun.* **2009**, *180*, 2582−2615.

(36) Gonze, X. A Brief Introduction to the ABINIT Software Package. *Z. Kristallogr. - Cryst. Mater.* **2005**, *220*, 558−562.

(37) Perdew, J. P.; Burke, K.; Ernzerhof, M. Generalized Gradient Approximation Made Simple. *Phys. Rev. Lett.* **1996**, *77*, 3865.

(38) Blöchl, P. E. Projector Augmented-Wave Method. *Phys. Rev. B* **1994**, *50*, No. 17953.

(39) Grimme, S. Semiempirical GGA-Type Density Functional Constructed with A Long-Range Dispersion Correction. *J. Comput. Chem.* **2006**, *27*, 1787−1799.

(40) Henkelman, G.; Uberuaga, B. P.; Jónsson, H. A Climbing Image Nudged Elastic Band Method for Finding Saddle Points and Minimum Energy Paths. *J. Chem. Phys.* **2000**, *113*, 9901−9904.

(41) Jing, Y.; Zhou, Z.; Cabrera, C. R.; Chen, Z. Metallic VS_2 Monolayer: A Promising 2D Anode Material for Lithium Ion Batteries. *J. Phys. Chem. C* **2013**, *117*, 25409−25413.

(42) Zhu, Z.; Tománek, D. Formation and Stability of Cellular Carbon Foam Structures: An ab initio Study. *Phys. Rev. Lett.* **2012**, *109*, No. 135501.

(43) Shi, L.; Zhao, T. S.; Xu, A.; Xu, J. B. Ab initio Prediction of a Silicene and Graphene Heterostructure as An Anode Material for Li- and Na-Ion Batteries. *J. Mater. Chem. A* **2016**, *4*, 16377−16382.

(44) Xu, J.; Wang, M.; Wickramaratne, N. P.; Jaroniec, M.; Dou, S.; Dai, L. High-Performance Sodium Ion Batteries Based on a 3D Anode from Nitrogen-Doped Graphene Foams. *Adv. Mater.* **2015**, *27*, 2042−2048.

(45) Er, D.; Detsi, E.; Kumar, H.; Shenoy, V. B. Defective Graphene and Graphene Allotropes as High-Capacity Anode Materials for Mg Ion Batteries. *ACS Energy Lett.* **2016**, *1*, 638−645.

(46) Mukherjee, R.; Thomas, A. V.; Datta, D.; Singh, E.; Li, J.; Eksik, O.; Shenoy, V. B.; Koratkar, N. Defect-Induced Plating of Lithium Metal within Porous Graphene Networks. *Nat. Commun.* **2014**, *5*, No. 3710.

(47) Jing, Y.; Zhou, Z. Computational Insights into Oxygen Reduction Reaction and Initial Li_2O_2 Nucleation on Pristine and N-Doped Graphene in $Li−O_2$ Batteries. *ACS Catal.* **2015**, *5*, 4309−4317.

(48) Guo, D.; Shibuya, R.; Akiba, C.; Saji, S.; Kondo, T.; Nakamura, J. Active Sites of Nitrogen-Doped Carbon Materials for Oxygen Reduction Reaction Clarified Using Model Catalysts. *Science* **2016**, *351*, 361−365.

(49) Jiang, K.; Eitan, A.; Schadler, L. S.; Ajayan, P. M.; Siegel, R. W.; Grobert, N.; Mayne, M.; Reyes-Reyes, M.; Terrones, H.; Terrones, M. Selective Attachment of Gold Nanoparticles to Nitrogen-Doped Carbon Nanotubes. *Nano Lett.* **2003**, *3*, 275−277.

(50) Liang, H. W.; Wei, W.; Wu, Z. S.; Feng, X.; Müllen, K. Mesoporous Metal-Nitrogen-Doped Carbon Electrocatalysts for Highly Efficient Oxygen Reduction Reaction. *J. Am. Chem. Soc.* **2013**, *135*, 16002−16005.

(51) Tang, Y.; Allen, B. L.; Kauffman, D. R.; Star, A. Electrocatalytic Activity of Nitrogen-Doped Carbon Nanotube Cups. *J. Am. Chem. Soc.* **2009**, *131*, 13200−13201.

(52) Mawhinney, D. B.; Naumenko, V.; Kuznetsova, A.; Yates, J. T., Jr.; Liu, J.; Smalley, R. E. Surface Defect Site Density on Single Walled Carbon Nanotubes by Titration. *Chem. Phys. Lett.* **2000**, *324*, 213−216.

(53) Hao, F.; Fang, D.; Xu, Z. Mechanical and Thermal Transport Properties of Graphene with Defects. *Appl. Phys. Lett.* **2011**, *99*, No. 041901.

(54) Okamoto, Y. Density Functional Theory Calculations of Alkali Metal (Li, Na, and K) Graphite Intercalation Compounds. *J. Phys. Chem. C* **2014**, *118*, 16−19.

(55) Wu, M.; Wu, X.; Pei, Y.; Wang, Y.; Zeng, X. C. Three-Dimensional Network Model of Carbon Containing Only sp^2-Carbon Bonds and Boron Nitride Analogues. *Chem. Commun.* **2011**, *47*, 4406−4408.

(56) Zhang, J.; Xiong, Q. Negative Poisson's Ratio in Graphene-Based Carbon Foams. *Phys. Chem. Chem. Phys.* **2018**, *20*, 4597−4605.

(57) Han, Y.; Yang, J. Y.; Hu, M. Unusual Strain Response of Thermal Transport in Dimerized Three-Dimensional Graphene. *Nanoscale* **2018**, *10*, 5229−5238.

(58) Gao, X.; Shen, X. Face-to-Face Crosslinking of Graphdiyne and Related Carbon Sheets toward Integrated Graphene Nanoribbon Arrays. *Carbon* **2017**, *125*, 536−543.